Geomechanics and Engineering, *Vol. 32, No. 3 (2023) 307-319*
https://doi.org/10.12989/gae.2023.32.3.307

Shaking table test on seismic response and failure characteristics of ground fissures site during earthquakes

Chao Zhang[1,2a], Xuzhi Nie*[1,2], Zhongming Xiong[3], Yuekui Pang[1,2], Xiaolu Yuan[4], Yan Zhuge[5] and Youjun Xu[1,2]

[1]*School of Civil Engineering, Inner Mongolia University of Science & Technology, Baotou 014010, China*
[2]*Academician Workstation of Mine Safety and Underground Engineering, Inner Mongolia University Science and Technology, Baotou 014010, China*
[3]*School of Civil Engineering, Xi'an University of Architecture & Technology, Xi'an 710055, China*
[4]*School of Materials and Metallurgy, Inner Mongolia University of Science & Technology, Baotou 014010, China*
[5]*School of Natural & Built Environments, University of South Australia, Adelaide, 5108, Australia*

(*Received May 15, 2022, Revised January 4, 2023, Accepted January 13, 2023*)

Abstract. Ground fissures have a huge effect on the integrity of surface structures. In high-intensity ground fissure regions, however, land resource would be wasted and city building and economic development would be limited if the area avoiding principle was used. In view of this challenge, to reveal the seismic response and seismic failure characteristics of ground fissure sites, a shaking table test on model soil based on a 1:15 scale experiment was carried out. In the test, the spatial distribution characteristics of acceleration response and Arias intensity were obtained for a site exposed to earthquakes with different characteristics. Furthermore, the failure characteristics and damage evolution of the model soil were analyzed. The test results indicated that, with the increase in the earthquake acceleration magnitude, the crack width of the ground fissure enlarged from 0 to 5 mm. The soil of the hanging wall was characterized by earlier cracking and a higher abundance of secondary fissures at 45°. Under strong earthquakes, the model soil, especially the soil near the ground fissure, was severely damaged and exhibited reduced stiffness. As a result, its natural frequency also decreased from 11.41 Hz to 8.05 Hz, whereas the damping ratio increased from 4.8% to 9.1%. Due to the existence of ground fissure, the acceleration was amplified to nearly 0.476 m/s^2, as high as 2.38 times of the input acceleration magnitude. The maximum of acceleration and Arias intensity appeared at the fissure zone, which decreased from the main fissure toward both sides, showing hanging wall effects. The seismic intensity, duration and frequency spectrum all had certain effects on the seismic response of the ground fissure site, but their influence degrees were different. The seismic response of the site induced by the seismic wave that had richer low-frequency components and longer duration was larger. The discrepancies of seismic response between the hanging wall and the footwall declined obviously when the magnitude of the earthquake acceleration increased. The research results will be propitious to enhancing the utilizing ratio of the limited landing resource, alleviation of property damages and casualties, and provide a good engineering application foreground.

Keywords: ground fissure; seismic failure characteristics; seismic response; shaking table test; soil damage

1. Introduction

Ground fissures are widely distributed all over the world, such as in China, America, Mexico, Turkey, Greece, Ethiopia, etc. (Holzer 1984, Pacheco-Martínez *et al*. 2013, Sancio *et al*. 2002, Kalogirou *et al*. 2014, Wang *et al*. 2010, Ayalew *et al*. 2004, Stacey and Bell 1999). They present a major urban geohazard threatening human life and influencing construction security. Since the first description in 1958, more than 6000 ground fissures have been reported in China alone (Zhang 1990). Among them, 212 ground fissures are distributed over 20 counties and cities around the Fen-wei Basin (Peng *et al*. 2020). These have caused serious harm to civil construction, including damaged buildings, distorted roads and ruptured pipelines, severely limiting landing resource and restricting city construction in this area.

In the economic and cultural center of Northwest China, Xi'an, 14 ground fissures have been identified, covering an area of 150 km^2 (Liu *et al*. 2021). The complex geological environment (loess erosion, ground fissures and earthquakes) brings considerable engineering challenges to the ongoing Xi'an metro project. Besides, the activity of a main fissure or the appearance of secondary fissures increases the possibility of failure in existing buildings, and raises the difficulty of ancient building protection (Peng *et al*. 2020). As a result, many historic buildings have suffered destruction to varying degrees (Fig. 1).

Recently, many studies on the geological characteristics of ground fissure have been carried out, including the formation mechanism, spatial distribution and development regularities (Zhang 1990, Peng *et al*. 2020, Liu *et al*. 2021, Wan *et al*. 2020, Wang *et al*. 2020). There have been two

*Corresponding author, M.Eng.
E-mail: nie2568828101@126.com
[a]Ph.D.
E-mail: z_dynasty@126.com

ISSN: 2005-307X (Print), 2092-6219 (Online)

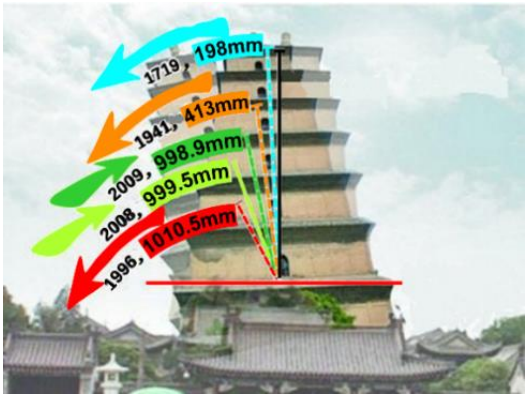

(a) Dayan Pagoda leaning at an angle (Zhang 1990)

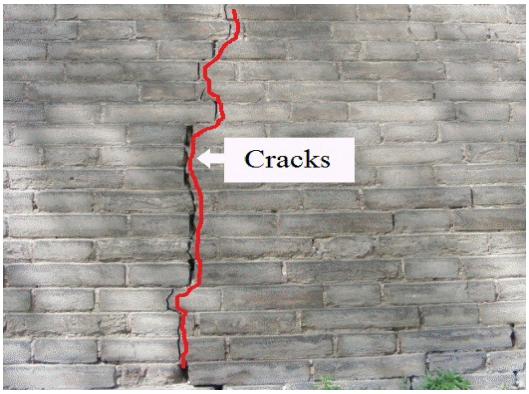

(b) Cracking in the Xi'an Circumvallation

Fig. 1 Destruction of ancient architectures

different viewpoints regarding the formation mechanism. According to the first one, ground fissure formation stems from excessive groundwater pumping (Holzer 1984, Pacheco-Martínez *et al*. 2013). The second concerns tectonic movement underneath as the main reason for ground fissure formation (Ayalew *et al*. 2004). Recently, an increasing number of researchers have agreed that the formation of ground fissures is directly caused by overexploited underground resources, and their distribution is determined by their tectonic structure (Peng *et al*. 2020, Wang *et al*. 2020). In terms of the spatial distribution and development regularities of ground fissures, Peng *et al*. (2020) provided a detailed study in Xi'an, and found that they had clearly uniform directions from NE to SW, parallel to the fault strike. Wang *et al*. (2000) investigated ground fissure distribution in several typical urban zones (such as Handan, Tai'an, Datong and Linfen), and projected a series of protection measures to minimize the damage caused by ground fissures.

Some scholars conducted model tests and microtremor analyses to investigate the dynamic response of ground fissure sites (Liu *et al*. 2018, Liu *et al*. 2019, Xiong *et al*. 2020, Hu *et al*. 2014, Wang *et al*. 2015). Liu *et al*. (2018, 2019) carried out a shaking table model test to simulate the seismic response of the ground with hidden fissures in the region of Xi'an, and revealed the distribution of acceleration in the site. Hu *et al*. (2014), Wang *et al*. (2015) and Xiong *et al*. (2020) respectively carried out shaking table tests to explore the acceleration response on different

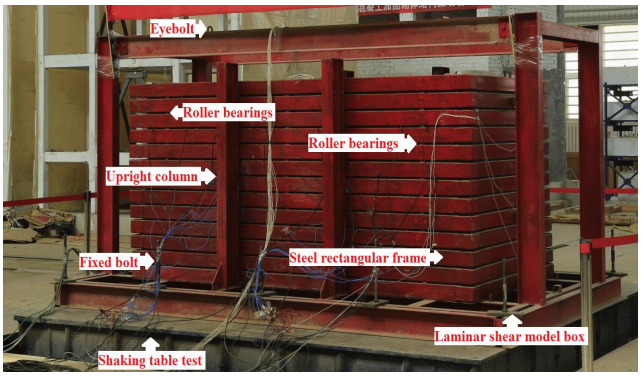

Fig. 2 Laminar soil box

types of sites with ground fissures. The acceleration response law of the primary and secondary fissures of the site with "y" type ground fissure was obtained. The peak ground acceleration (PGA) of the soil in the hanging wall was greater than that in the footwall. The PGA near the ground fissure was evidently amplified due to the existence of ground fissure. Chang *et al*. (2020) and You *et al*. (2021) revealed the acceleration characteristics of a site with ground fissures in the Linfen and Datong basins through microtremor measurement. However, apart from the above works, tests or numerical simulation analyses of the seismic response and failure characteristics of sites with ground fissures in high-intensity Xi'an areas have been scarce. These literatures only revealed the distribution law of acceleration response in the ground fissure site, and did not analyze the seismic response of the ground fissure site under different ground motion parameters, such as seismic intensity, duration and frequency spectrum.

In view of the above, taking a site with f_4 ground fissures in Xi'an as the prototype, the seismic response and failure characteristics were systematically investigated by a shaking table test. The research results will be beneficial to enhancing the utilizing ratio of the limited landing resource, alleviation of property damages and casualties, and provide a good engineering application basis.

2. Experimental design

2.1 Testing apparatus

In the test, the seismic excitation of the model was performed by using a shaking table. A laminar shear box (Fig. 2) was developed and utilized for the placement of model soil, which had a high stiffness to ensure that no deformation could occur during vibration. Meanwhile, to effectively simulate the shearing deformation of soil along the longitudinal direction during strong earthquakes, roller bearings were placed between the two frames to reduce frictional resistance. The main technical parameters of the testing apparatus are shown in Table 1 below.

The bearing capacity of the loading device determines that the geotechnical model has to fit in the box within finite boundaries. The boundaries (friction boundary, slip boundary and flexible boundary) of the box may generate

Table 1 Main technical parameters of the testing apparatus

Instrument	Main performance	Parameters	Main performance	Parameters		
Shaking table	Platform size	4.0 m×4.0 m	Maximum horizontal acceleration	Direction	X	±1.2 g
	Maximum load	30 t			Y	±0.8 g
	Frequency range	0.1~50 Hz	Maximum displacement		X	±15 cm
	Maximum tilting moment	80 t·m			Y	±25 cm
	Maximum eccentric bending moment	30 t·m	Maximum speed		X	±100 cm/s
	Maximum eccentricity	0.6 m			Y	±125 cm/s
Laminar shear model box	Internal dimensions	3.0 m×1.5 m	Height of single steel frame	0.12 m		
	External dimensions	3.2 m×1.7 m	Number of single steel frame	13		
Accelerometer	Measuring range	±1.5 g	Frequency range	0.1~50 Hz		
Displacement meter	Maximum displacement	300 mm	Resolution	0.03%		

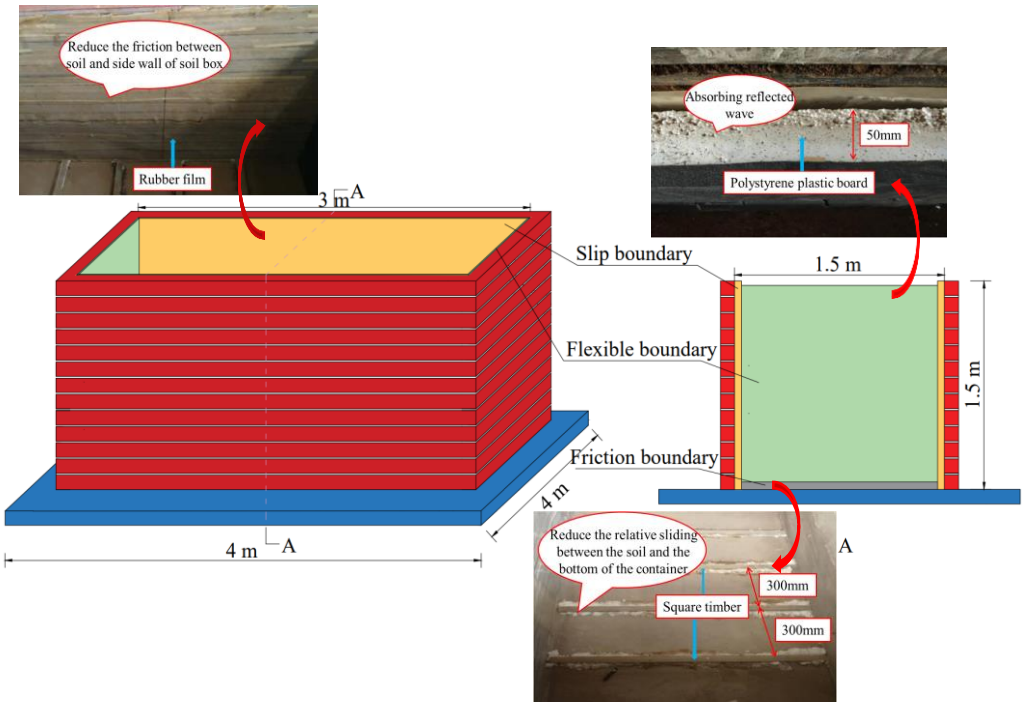

Fig. 3 Detailed arrangement of the boundary

reflected waves that are not present in the prototype when seismic waves propagate in the model soil (Lee *et al*. 2012). Thus, before making models, a series of measures should be taken to reduce the boundary effect (Zhu *et al*. 2022, Dong *et al*. 2020), as shown in Fig. 3.

2.2 Similarity ratio

In large-scale dynamic model tests of geotechnical engineering, it is necessary to determine the geometric, physical and mechanical similarities for the simulation of the actual site condition (Lu and Chen 2001). According to the structural features of the study site with ground fissures, the loading capability and performance of shaking table, the volume and boundary effect of the box, the model construction technology, and some other factors, the geometrical similarity ratio of the model was set as 1:15. The similarity ratios of the test model are shown in Table 2.

2.3 Model soil and material properties

A site with f_4 ground fissures was used as the testing prototype. It is divided by ground fissure dipped at 80° into two parts, named as the hanging wall and the footwall. The width of ground fissure is generally 1-80 mm. The extension of this fissure is up to 11.5 km long, and many branch fissures are usually developed alongside the main fissure, forming a fracture zone that is typically 8-10 m in width (Peng *et al*. 2020, Lee *et al*. 1996). Based on the characteristics of the site with ground fissures in Xi'an and the loading capability of the test system, a geological model was established, with the dimensions of 3.0×1.5×1.5

Table 2 Similarity ratios of the test model

Type	Physical quantity	Similarity ratios	Physical quantity	Similarity ratios
Geometry properties	Length l	S_l=0.0667		
Material properties	Equivalent density ρ	S_ρ=1	Shear modulus G	S_G=0.1333
	Strain ε	S_ε=1	Internal friction angle φ	S_φ=1
	Stress σ	S_σ=0.1333	Poisson's ratio μ	S_μ=1
	Elastic modulus E	S_E=0.1333	Cohesion c	S_c=0.1333
	Water content w	S_w=1		
Dynamic properties	Dynamic displacement d	S_d=0.0667	Acceleration a	S_a=2
	Duration t	S_t=0.1826	Frequency f	S_f=5.4772

Table 3 Physical and mechanical properties of the testing model

Soil	Water content (%)	Natural density (kg/m^3)	Cohesion (kPa)	Internal friction angle (°)	Compression modulus (MPa)	Shear modulus (MPa)	Elastic modulus (MPa)	Poisson's Ratio
Loess	23.5	1.71	48	27.6	8.01	110.49	39.48	0.34
Paleosol	22.9	1.82	49	27.3	6.72	139.45	49.83	0.34
Silty Clay	25.2	1.94	45	26.6	7.07	163.34	58.37	0.34
mixture	28.3	2.19	6	19.2	20.32	130.67	46.70	0.30

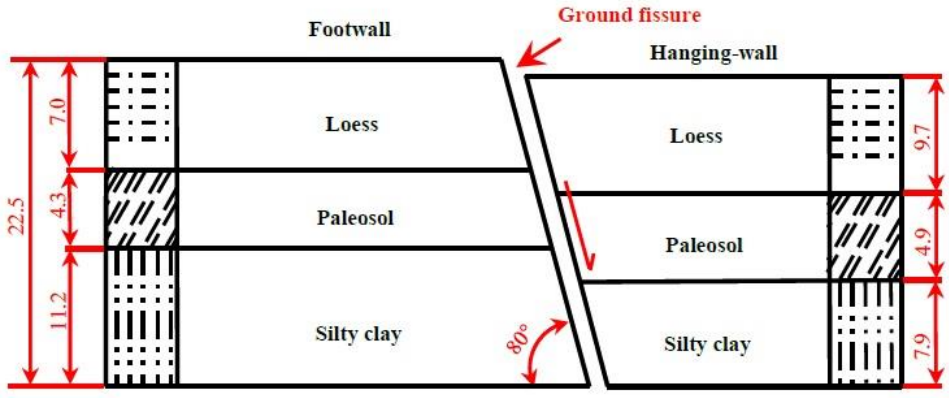

Fig. 4 Section structural characteristics of the site with ground fissures (unit: m)

meters. The prototype site is shown in Fig. 4.

Based on the bandwidth of ground fissure and the geometrical similarity ratio, the fissure width was set as 2 cm. Mixtures of silver sand and hydrated lime were utilized for simulating the soil particles in the fissure (Liu *et al*. 2019, Xiong *et al*. 2020, Chang *et al*. 2020). The physical and mechanical properties of the testing model are listed in Table 3. When preparing the samples, the homogeneous soil samples near the f_4 ground fissure were used for making the model. To ensure uniform compaction, the soil samples were filled into the box and compacted to a solid layer by layer to a set height (20 cm). After each compaction step was completed, several samples of the remolded soil of each layer were collected to carry out indoor tests (Fig. 5), in order to control for physical parameters (natural density, water content, strength and deformation parameters). The test model is shown in Fig. 6.

Fig. 5 Indoor direct shear and compaction tests

2.4 Instrumentation

Sensors including 41 accelerometers and 5 displacement meters were used in the shaking table test to record various parameters at different positions. The performance indices

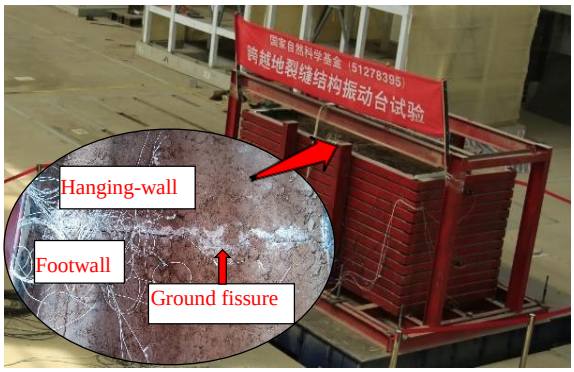

Fig. 6 Testing model

(a) Accelerometers

(b) Displacement meters

(c) Data acquisition systems

Fig. 7 Testing instrumentation and data acquisition equipment

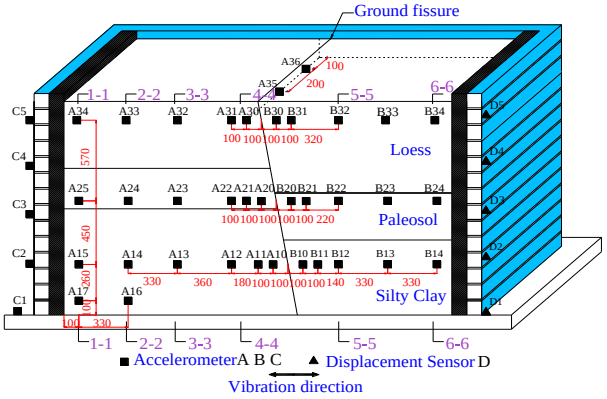

Fig. 8 Layout of sensors (Unit: mm)

of the accelerometers (Fig. 7(a)) and displacement meters (Fig. 7(b)) are shown in Table 1. The data were tested and collected in real time by a data acquisition system, and the sampling frequency was 100 Hz (Fig. 7(c)).

According to a previous computational analysis on the dynamic response of the site with ground fissures (Xiong *et al*. 2020), the accelerometers were laid in three soil layers, mainly distributed near the ground fissure, to study the change rule of ground motion parameters in the soil, as shown in Fig. 8. Among them, accelerometers buried in the footwall side were denoted as A_{ij}, and those buried in the hanging wall side were denoted as B_{ij}. All of the accelerometers were housed in waterproof boxes.

2.5 Ground motion records

When the aim is to explore the seismic response under different seismic waves, the input seismic waves should contain different spectral characteristics and strong motion duration. Consequently, typical seismic records (Jiangyou, El Centro and Cape Mendocino) were chosen for the simulation of a large earthquake excitation in the test. The first two seismic waves were collected from the seismological station on the surface, whereas the Cape Mendocino wave that has richer high-frequency components was collected from the bedrock. The spectral characteristics of the three seismic waves are shown in Fig. 9.

During the test, it was necessary to consider the failure characteristics of the site under the action of different seismic intensities. Thus, the peak ground accelerations of these seismic waves were adjusted according to 7 test stages from 0.10 g to 1.20 g, respectively, as listed in Table 4. Among them, WN stands for white noise; JY stands for Jiangyou wave; EL stands for El Centro wave; and CM stands for Cape Mendocino wave. These curves were compressed according to the time similarity ratio (S_t=0.1826) in the shaking table test. White noise was selected as input excitation after each test stage to observe the modal characteristics of the site.

3. Seismic failure characteristics of the site with ground fissures

3.1 Macroscopic failure mode

The macroscopic failure evolution process of the site with ground fissures was observed during strong earthquakes, as shown in Fig. 10. The failure characteristics of the site after loading at each stage are shown in Fig. 11 below.

Before the test, the ground fissure was in a closed state, as it was completely filled with a mixture of silver sand and hydrated lime. Under 0.10 g PGA, as a result of the main fissure being partially cracked, there was a stress concentration zone at the fissure. Meanwhile, some of the mixture outflowed from the fissure due to the mutual extrusion of hanging wall and footwall (Fig. 11(a)).

Under 0.20 g PGA, the crack width increased further, and the crack length was gradually extended. More mixture was observed in the surface near the fissure zone (Fig. 11(b)).

Under 0.40 g PGA, some secondary fissures at 45° developed on the hanging wall alongside the main fissure, and the crack width of the main fissure increased further.

Under 0.60 g PGA, the number of secondary fissures of the hanging wall side increased, and the same kind of secondary fissures were observed on the footwall (Fig. 11(c)).

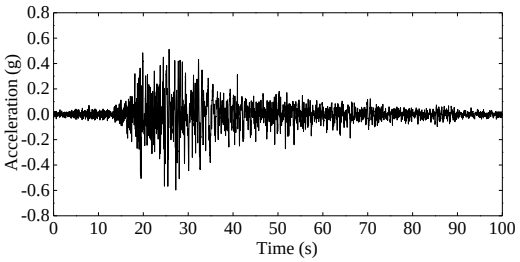

(a) Jiangyou wave

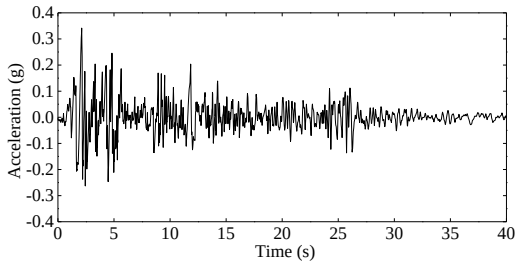

(b) El Centro wave

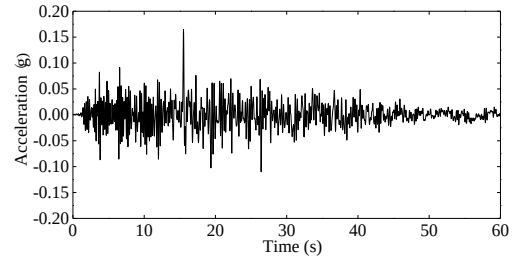

(c) Cape Mendocino wave

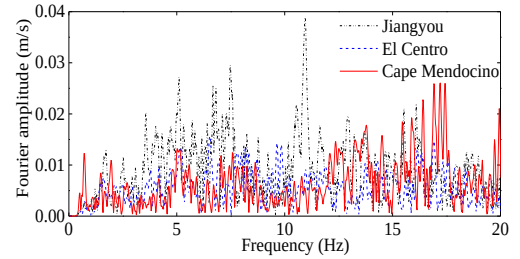

(d) Fourier spectra of three waves

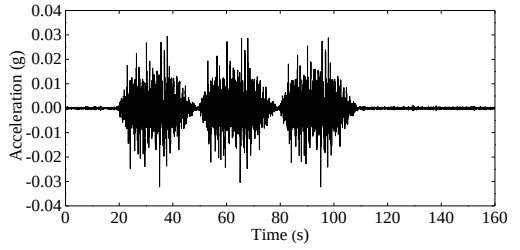

(e) White noise

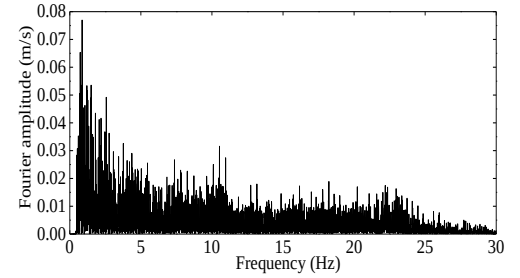

(f) Fourier spectra of white noise

Fig. 9 Spectral characteristics of seismic waves and white noise

When the test was complete, the maximum crack width of the main fissure was up to 5 mm (Fig. 11(d)). In addition, the trend of the main fissure in the paleosol layer had evidently shifted by 19 mm from the initial position along the vibration direction, and the width of main fissure in the paleosol layer had narrowed from 20 mm to 13 mm (Fig. 11(e)). Moreover, the paleosol soil of the footwall had invaded into the hanging wall (Fig. 11(f)).

3.2 Seismic damage

Marginal spectrum is the integral of Hilbert spectrum on the time axis, which can reflect the contribution of signal frequency to energy amplitude (Cao *et al*. 2017), and can be utilized to evaluate the damage development in soil (Huang *et al*. 2018). To date, the marginal spectrum theory has been applied to the damage detection of slope soil (Cao *et al*. 2017, Huang *et al*. 2018, Wei *et al*. 2010, Dong *et al*. 2008), so that the stability and energy change law of slope soil can be analyzed, and the damage characteristics of reinforced slope can be studied. Therefore, in this paper, the damage development in the soil of the site with ground fissures was discussed through the marginal spectrum theory.

Before the loading test, the model soil was undamaged; therefore, the result of 1st white noise sweep (WN-1 condition) before the loading was selected as the benchmark. The damage index calculated by the Hilbert marginal spectrum was normalized, so as to more clearly display the damage degree of each measuring point. At the same time, a new damage index d_i was defined as

$$d_i = 1 - \frac{DI_i}{DI_1} \tag{1}$$

where DI_1 represents the damage coefficient corresponding to each measuring point under the WN-1 condition, and $DI_i (i=2,\ldots,7,8)$ denotes the damage coefficient corresponding to the 2nd-8th white noise sweep (WN-2 to WN-8) of each measuring point. There is a positive correlation between the damage degree of soil and the damage index.

In order to explore the damage development of soil at different positions on either side of the ground fissure, the surface observation data were calculated through Formula (1), and the test results were plotted in Fig. 12.

According to the analysis in Fig. 12, during earthquakes, the soil near the ground fissure suffered the most serious damage, and the damage index decreased with the distance from the fissure. Besides, the damage degree of soil on the hanging wall was greater than that at the symmetrical position of the footwall. The damage degree of the model soil gradually intensified, and the growth of damage index steadily slowed down as the magnitude of the earthquake acceleration increased.

By observing the test phenomena, it was found that the formation of soil cracks in the hanging wall occurred earlier, and these had greater width and length. Moreover, the number of secondary fissures recorded on the hanging wall side was higher than that on the other side. The cracking phenomenon of soil near the ground fissure was more prominent, which was consistent with the above law in the site with ground fissures.

Table 4 Test scenarios

Test sequence	Loading condition	PGA (g)	Duration(s)	Test sequence	Loading condition	PGA (g)	Duration(s)
1	WN-1	0.05	170	17	WN-5	0.05	170
2	JY-1	0.10	102	18	JY-5	0.60	102
3	EL-1	0.10	40	19	EL-5	0.60	40
4	CP-1	0.10	60	20	CP-5	0.60	60
5	WN-2	0.05	170	21	WN-6	0.05	170
6	JY-2	0.20	102	22	JY-6	0.80	102
7	EL-2	0.20	40	23	EL-6	0.80	40
8	CP-2	0.20	60	24	CP-6	0.80	60
9	WN-3	0.05	170	25	WN-7	0.05	170
10	JY-3	0.30	102	26	JY-7	1.20	102
11	EL-3	0.30	40	27	EL-7	1.20	40
12	CP-3	0.30	60	28	CP-7	1.20	60
13	WN-4	0.05	170	29	WN-8	0.05	170
14	JY-4	0.40	102	30	CP-8	0.30	13
15	EL-4	0.40	40	31	CP-9	0.30	8
16	CP-4	0.40	60	32	CP-10	0.30	4.5

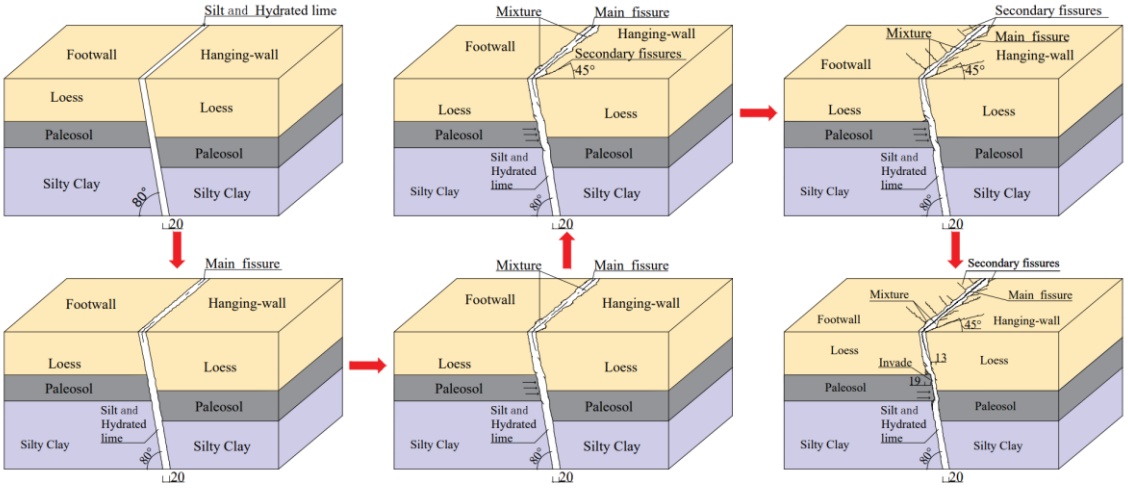

Fig. 10 Seismic failure evolution process of the ground fissure site

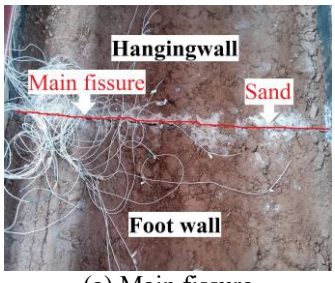

(a) Main fissure

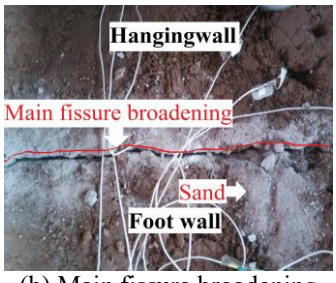

(b) Main fissure broadening

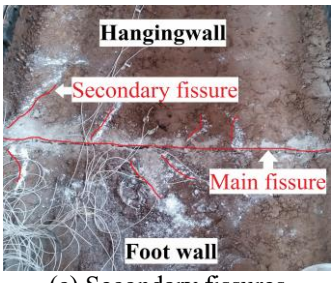

(c) Secondary fissures

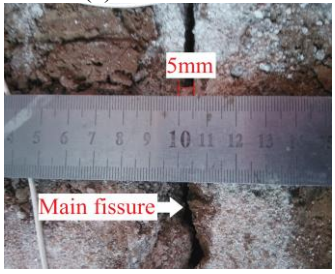

(d) Crack width

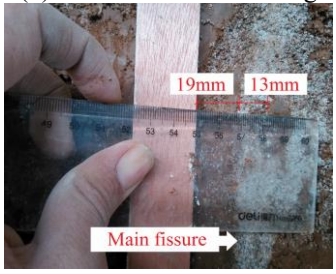

(e) Main fissure migration

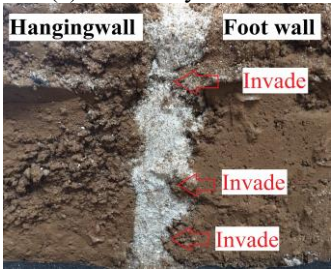

(f) Invasion

Fig. 11 Seismic failure characteristics of the ground fissure site

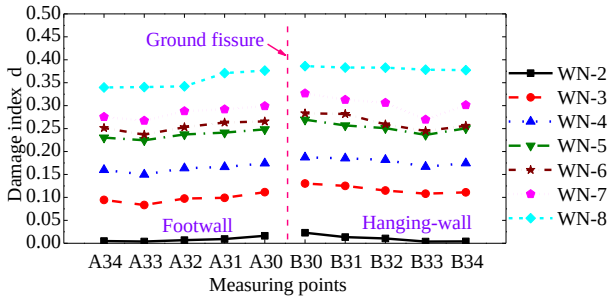

Fig. 12 Damage index on the ground surface under strong earthquakes

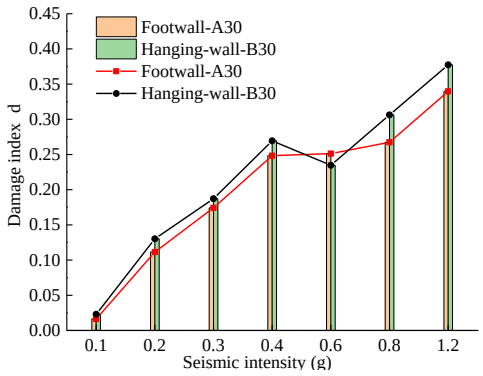

Fig. 13 Damage index under different input seismic intensities

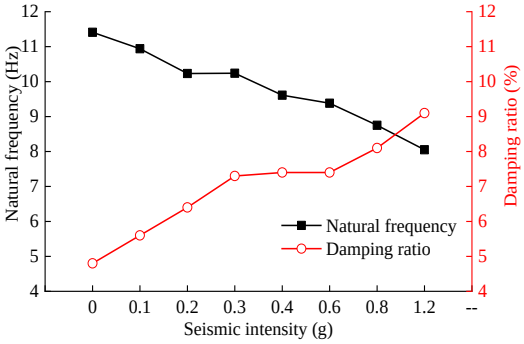

Fig. 14 Frequency and damping ratios of the soil

3.3 Modal characteristics

The relationships between the damage index on the ground surface and the seismic intensity are shown in Fig. 13. The modal characteristics of the testing model were determined by a frequency sweep test (from WN-1 to WN-8), as shown in Fig. 14.

As seen from Figs. 13 and 14, with the increase in seismic intensity, the model soil was severely damaged and its stiffness decreased. As a result, its natural frequency also linearly decreased from 11.41 Hz to 8.05 Hz, but the damping ratio increased from 4.8% to 9.1%, which shows that the softening of the model soil was more intense during strong earthquakes with higher peak ground acceleration (Xiong *et al*. 2018). The change trend of damping ratio of the site with ground fissures was in accordance with the trend of damage index in the hanging wall and the footwall, which increased approximately in an inverse "S-shape".

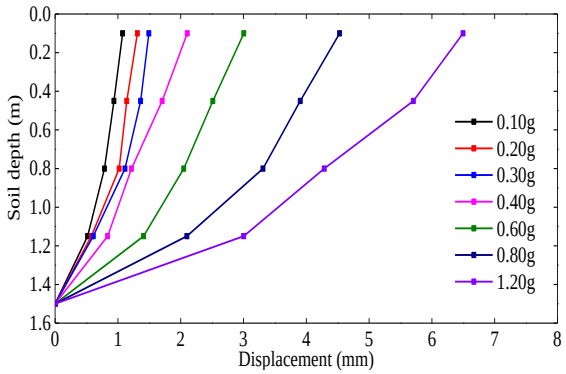

Fig. 15 Horizontal displacement response

4. Seismic response of the site with ground fissures

4.1 Horizontal displacement response

Fig. 15 shows the envelope diagram of relative displacement of the D2-D5 measuring points outside the laminar shear box. It can be seen that the displacement responses of the test model in the horizontal direction are consistent under earthquakes with different intensities. The peak displacement gradually increases with the thickness of soil layer, and the soil deformation is shear deformation. The displacement at the same location increases with the elevation of input earthquake intensity. The above rules show that the laminar shear box can truly simulate the shear deformation characteristics of foundation soil under the action of earthquake.

4.2 Amplification effect on the ground surface

Arias intensity (I_a), an index of earthquake intensity, is defined as the sum of the energies dissipated per unit weight by a population of oscillators with resonant frequencies ranging from zero to infinity (Arias 1970). It is closely related to collapse, landslides, and ground fissure caused by earthquakes and other geohazards. Compared to other indices, it has the advantage of being more objective and reasonable in describing a single earthquake (Harp and Wilson 1995). The Arias intensity is defined as:

$$I_a = \frac{\pi}{2g}\int_0^{T_d} a^2(t)dt \tag{2}$$

where $a(t)$ represents the acceleration time histories; g denotes the gravitational acceleration; T_d is the seismic duration.

The amplification factors of peak ground acceleration and Arias intensity are shown in Fig.16. It was found that the PGA and I_a recorded on the surface of the hanging wall side were about 1.05~1.22 times larger than those recorded on the other side, which confirms the test phenomena in that the damage of hanging wall was more severe than that of the footwall, exhibiting remarkable hanging wall effects. Due to the existence of ground fissure, the acceleration of B30 and A30 was respectively amplified to nearly 0.476 m/s^2 and 0.424 m/s^2, that is, as high as 2.38 and 2.12 times the input acceleration magnitude.

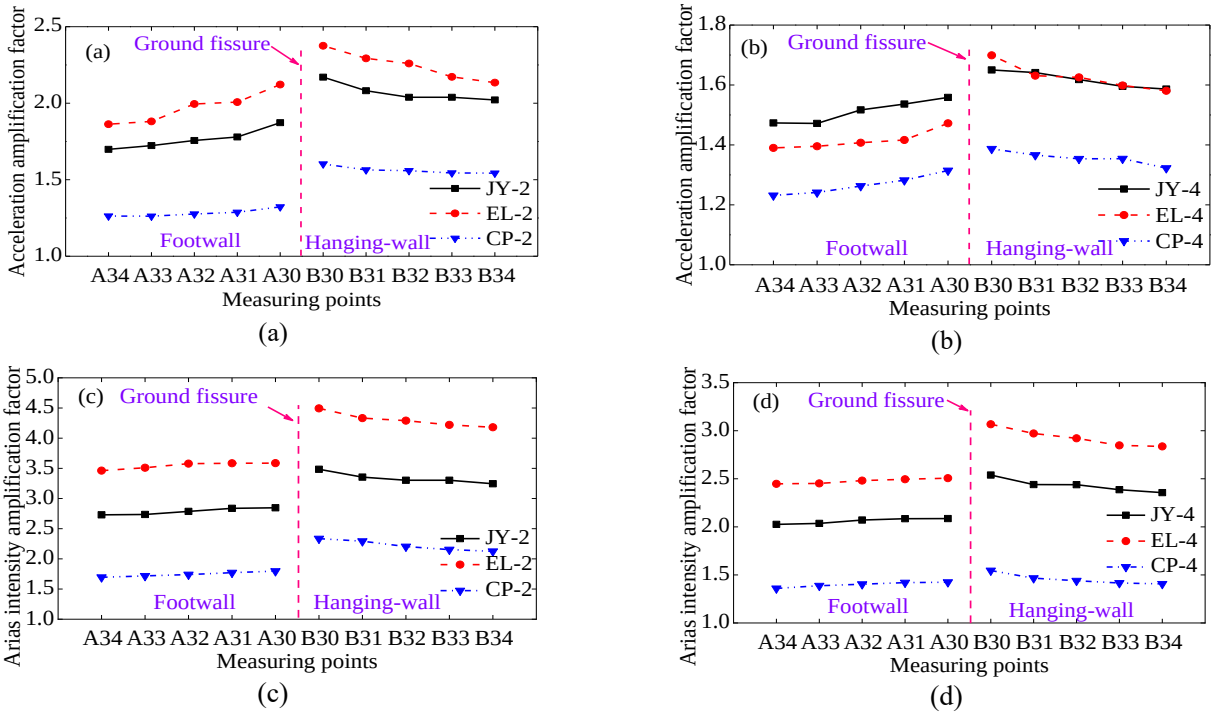

Fig. 16 Amplification factor on the ground surface: (a) PGA under 0.2 g, (b) PGA under 0.4 g, (c) I_a under 0.2 g and (d) I_a under 0.4 g

The maximum of acceleration and Arias intensity appeared at the fissure zone. When the measuring position of the accelerometer was far from the ground fissure, the amplification factors decreased. The decreasing amplitude of the hanging wall was larger than that of the other side. The reason may be that the seismic wave was decomposed into a variety of transmitted and reflected waves at the ground fissure and formed a complex seismic wave field in a certain range around the fissure, owing to the effects on the properties and tectonic feature of the soil at the site. At the same time, the energy carried by seismic waves was mainly concentrated around the ground fissure. In a weak area of the entire soil, the energy is released more easily from the ground fissure.

4.3 Amplification effect under different seismic waves

Fig. 17 shows the variation trend of peak ground acceleration and Arias intensity amplification factors with increasing soil depth. It was found that, with the vertically propagated shear wave, the amplitude of seismic wave was increased by the thickness of soil layer. In other words, the amplification factors increased from the bedrock to the Earth's surface. However, owing to the nonlinear and strength softening characteristic of the soil, the values of PGA amplification factors recorded by the accelerometer A17 at the depth of 1.4 m were larger than those recorded by A15 at the depth of 1.14 m. These phenomena demonstrated that the damping effect of silty clay with higher water content was more intense for strong earthquakes. The values of I_a amplification factors recorded by A17 and A15 were less than 1.0, which also indicated that the soil with higher softness characteristics possessed improved energy dissipation capacity.

Furthermore, compared with the El Centro wave and Jiangyou wave with richer low-frequency components, the amplification factors under the action of Cape Mendocino wave were smaller. That is, the seismic response of the testing model was more vulnerable to the frequency components of strong earthquakes. For the same magnitude of earthquake acceleration, the seismic response became greater because the frequency component was closer to the natural frequency of the model soil.

4.4 Amplification effect under different seismic intensities

The relationships between the amplification factors and seismic intensity are shown in Fig. 18. Overall, the PGA and I_a amplification factors presented a decreasing trend with the increasing peak acceleration of the earthquake, and the decreasing amplitude of the measuring point on the hanging wall side was different from that on the other side. As the damping ratio increased from 4.8% to 9.1% with the seismic intensity, the ever-increasing energy dissipation capacity led to the difference in the amplification factor between the hanging wall and the footwall obviously diminish.

It is clearly seen from the figure that, when the input seismic intensity was in the range of 0.1 g-0.2 g, the decline rate of PGA and Arias amplification factor were the largest. Meanwhile, when the magnitude of the earthquake acceleration increased, the amplification factor suddenly decreased at a certain point, which might be caused by the

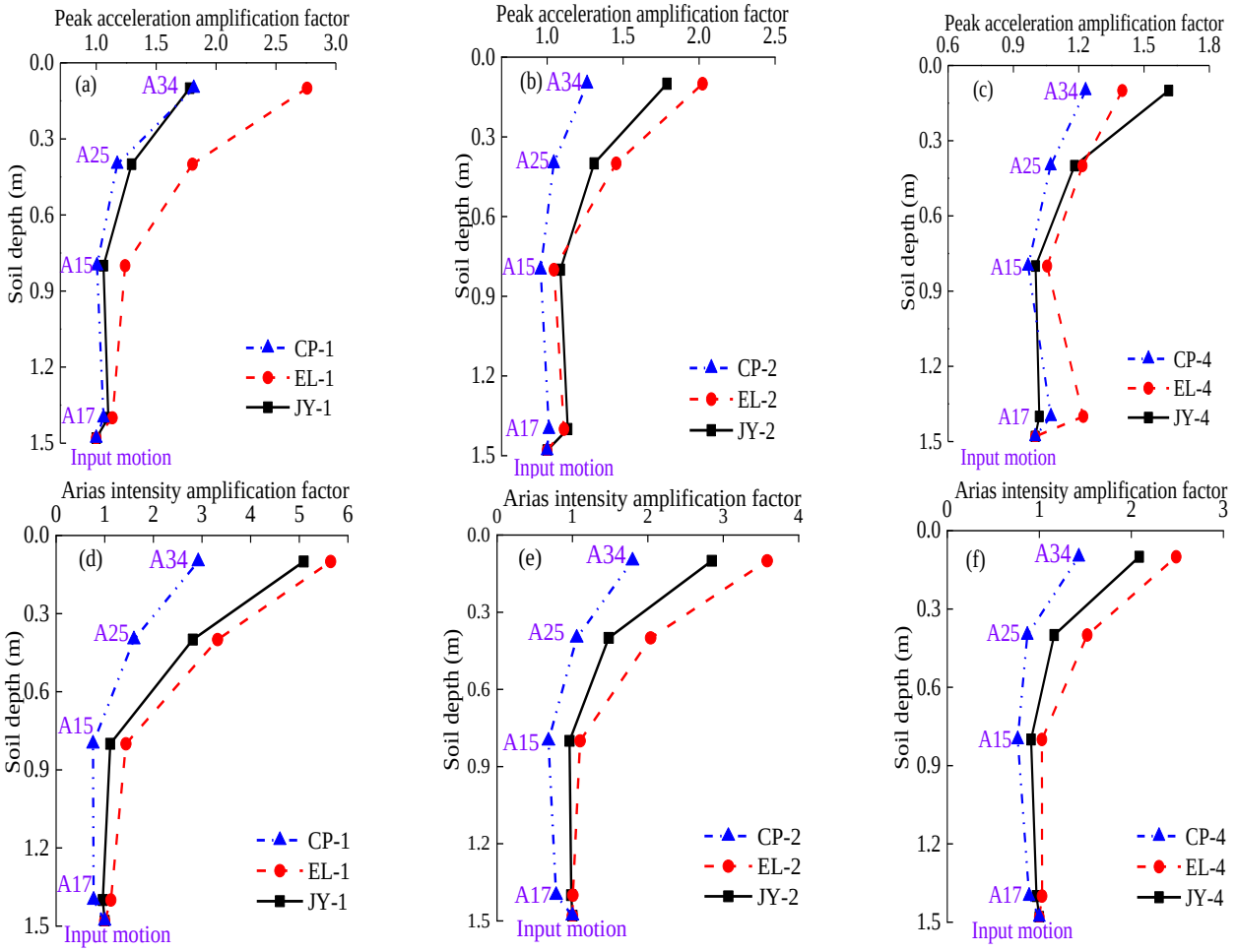

Fig. 17 Amplification factors for different soil depths: (a) PGA under 0.1 g, (b) PGA under 0.2 g, (c) PGA under 0.4 g, (d) I_a under 0.1 g, (e) I_a under 0.2 g and (f) I_a under 0.4 g

instability of seismic wave propagation due to the non-uniform decline of soil stiffness under certain conditions.

4.5 Amplification effect under different durations of strong earthquake

The amplification factors of PGA and I_a on the ground surface under the action of Cape Mendocino wave with different durations are shown in Fig. 19. It was found from the figure that the PGA and I_a recorded on the hanging wall were greater than those on the other side of the ground fissure, also exhibiting remarkable hanging wall effects. The amplification factor and its distribution range, as well as the energy release caused by the seismic wave with long duration were larger.

5. Conclusions

In this study, a 1:15 scale shaking table test was implemented to analyze the seismic response and seismic failure characteristics of a prototype site with ground fissures. The main conclusions derived from the test results are as follows:

- Under strong earthquakes, the crack width of the ground fissure enlarged from 0 to 5 mm with the increase in the earthquake acceleration magnitude, due to the concentration of seismic stresses at the fissure. The soil of the hanging wall cracked earlier, and the secondary fissures at 45° here were more abundant, which means that the soil damage on the hanging wall was more serious than that on the footwall.
- The model soil, especially the soil near the ground fissure, was severely damaged and suffered stiffness decrease, and the damage index decreased with the increasing distance from the fissure. As a result, its natural frequency also decreased from 11.41 Hz to 8.05 Hz, whereas the damping ratio increased from 4.8% to 9.1%.
- Due to the existence of ground fissure, the acceleration was amplified to nearly 0.476 m/s^2, as high as 2.38 times the input acceleration magnitude. The maximum of acceleration and Arias intensity appeared at the fissure zone, which decreased from the main fissure toward both sides, indicating hanging wall effects.
- The seismic intensity, duration and frequency spectrum

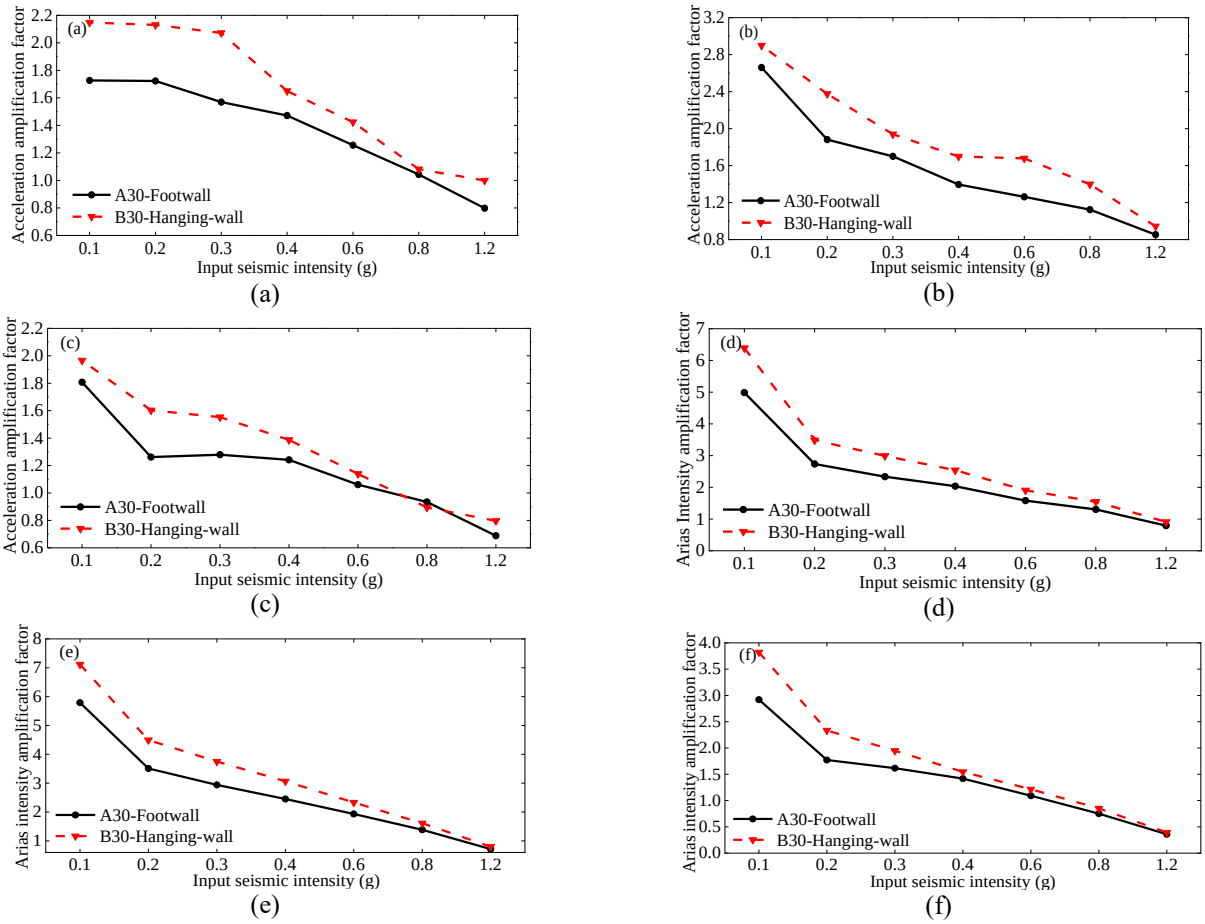

Fig. 18 Amplification factor under different seismic intensities: (a) PGA under Jiangyou wave, (b) PGA under El Centro wave, (c) PGA under Cape Mendocino wave, (d) I_a under Jiangyou wave, (e) I_a under El Centro wave and (f) I_a under Cape Mendocino wave

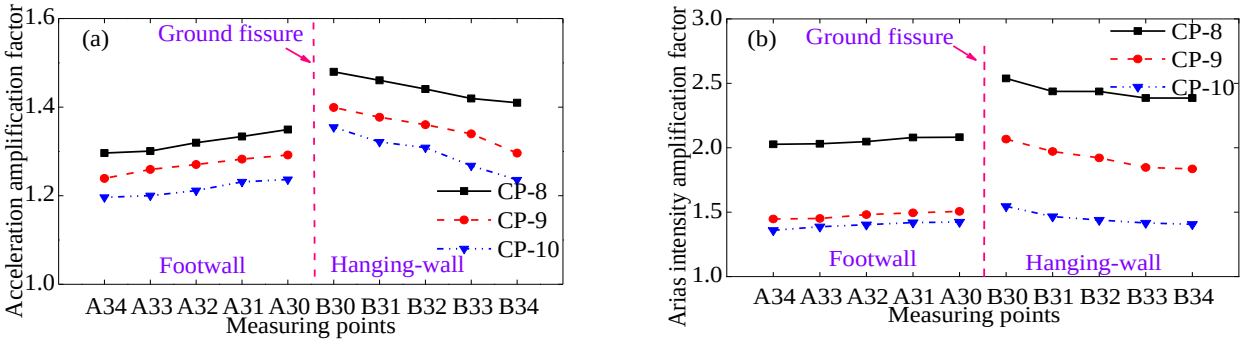

Fig. 19 Amplification factors under the action of Cape Mendocino wave with different durations: (a) PGA and (b) I_a

all had certain effects on the seismic response of the ground fissure site, while the amplification factors and their distribution ranges were different. Compared with the El Centro wave and Jiangyou wave with richer low-frequency components, the amplification factors under the action of Cape Mendocino wave were smaller. Furthermore, the seismic response was larger for the site with ground fissures caused by the seismic wave with longer duration.

- In conclusion, the existence of the ground fissure increased the level of damage of the model soil. The seismic waves reaching the ground surfaces of hanging wall and footwall were different, forming non-uniform seismic excitations. Therefore, it is necessary to reinforce the structure on the hanging wall during the stage of design and analysis.

Acknowledgments

The authors would like to express their gratitude to everyone who participated in the work of the Key Lab of Structure and Earthquake Rsistance in Xi'an University of Architecture and Technology for their support. Furthermore, we would like to thank the editors and reviewers for the helpful comments and revisions. This study was funded by the National Natural Science Foundation of China (Grant No. 51278399), National Natural Science Foundation of Inner Mongolia (No.2021bs05013), and the Science and Technology Project of Ministry of Housing and Urban-Rural Development of China (No.2019-k-044).

References

Ayalew, L, Yamagishi, H. and Reik, G. (2004), "Ground cracks in Ethiopian Rift Valley: facts and uncertainties", *Eng. Geol*., **75**(3), 309-324. https://doi.org/10.1016/j.enggeo.2004.06.018.

Arias, A. (1970), "A measure of earthquake intensity", (Ed., Hansen, R.J.), Seismic Design for Nuclear Power Plants, The M.I.T. Press, Cambridge, Britain: 438-489.

Chang, J., Deng, Y.H., Xuan, Y., Yan, Z.F., Wu, W. and He, J. (2020), "The dynamic response of sites with earth fissures as revealed by microtremor analysis-A case study in the Linfen Basin, China", *Soil Dyn. Earthq. Eng*., **132**(1-15). https://doi.org/10.1016/j.soildyn.2020.106076.

Lee, C.F., Zhang, J.M. and Zhang, Y.X. (1996), "Evolution and origin of the ground fissures in Xian, China", *Eng. Geol*., **43**(1), 45-55. https://doi.org/10.1016/0013-7952(95)00088-7.

Cao, L.C., Zhang, J.J., Liu, F.C., Liu, Y., Wu, J.B. and Wang, Z.J. (2017), "Seismic response and failure mode of the complex site with tilting strongly weathered layer and local slopes", *Chinese J. Rock Mech. Eng*., **36**(9), 2238-2250. (in Chinese) https://doi.org/10.13722/j.cnki.jrme.2017.0205.

Dong, Y.F., Li, Y.M., Xiao, M.K. and Lai, M. (2008), "Analysis of earthquake ground motions using an improved Hilbert–Huang transform", *Soil Dyn. Earthq. Eng*., **28**(1), 7-19. https://doi.org/10.1016/j.soildyn.2007.05.002.

Dong, J., Zhong, S., Wang, H.L. and Wu, Z.H. (2020), "Dynamic response characteristics of crossing tunnels under heavy-haul train loads", *Geomech. Eng*., **20**(2), 103-112. https://doi.org/10.12989/gae.2020.20.2.103.

Holzer, T.L. (1984), "Ground failure induced by ground-water withdrawal from unconsolidated sediment", *Rev. Eng. Geol*., VI: 67-105. https://doi.org/10.1130/REG6-p67.

Huang, T.L., Lou, M.L., Chen, H.P. and Wang, N.B. (2018), "An orthogonal Hilbert-Huang transform and its application in the spectral representation of earthquake accelerograms", *Soil Dyn. Earthq. Eng*., https://doi.org/10.1016/j.soildyn.2018.02.032.

Harp, E.L. and Wilson, R.C. (1995), "Shaking intensity thresholds for rock falls and slides: Evidence from the whittier narrows and superstition hills earthquake strong motion records", *Bull. Seismol. Soc. Am*., **85**(6), 1739-1757. https://doi.org/10.1785/BSSA0850061739.

Hu, Z.P., Wang, Q.Y., Luo, L.J., Ma, S.L. and Liu, A.L. (2014), "Shaking table test on seismic response difference between primary secondary ground fissures on sites with y-shape ground fissure", *China Civil Eng. J*., **47**(11), 98-107. (in Chinese) https://doi.org/10.15951/j.tmgcxb.2014.11.045.

Kalogirou, E.E., Tsapanos, T.M., Karakostas, V.G., Marinos, V.P. and Chatzipetros, A. (2014), "Ground fissures in the area of Mavropigi Village (N. Greece): Seismotectonics or mining activity?", *Acta Geophysica*, **62**(6), 1387-1412. https://doi.org/10.2478/s11600-014-0241-6.

Liu, R.C., Yang, C.S., Wang, Q.L. and Ji, L.Y. (2021), "Possible mechanism of the formation of the Jichechang ground fissure in Datong, China, based on in-situ observations", *Environ. Earth Sci*., **80**(14), 463. https://doi.org/10.1007/S12665-021-09715-2.

Liu, N.N., Huang, Q.B., Fan, W., Ma, Y.J. and Peng, J.B. (2018), "Seismic responses of a metro tunnel in a ground fissure site", *Geomech. Eng*., **15**(2), 775-781. https://doi.org/10.12989/gae.2018.15.2.775.

Liu, N.N., Feng, X.Y., Huang, Q.B., Fan, W. and Peng, J.B. (2019), "Dynamic characteristics of a ground fissure site", *Eng. Geol*., **248**, 220-229. https://doi.org/10.1016/j.enggeo.2018.12.003.

Lee, C.J., Wei, Y.C. and Kuo, Y.C. (2012), "Boundary effects of a laminar container in centrifuge shaking table tests", *Soil Dyn. Earthq. Eng*., **34**(1), 37-51. https://doi.org/10.1016/j.soildyn.2011.10.011.

Lu, X.L. and Chen, Y.Q. (2001), "Study on dynamic similitude theory of soil-structure interaction system", E*arthq. Eng. Eng. Vib*., **21**(3), 85-92. (in Chinese). https://doi.org/10.13197/j.eeev.2001.03.016.

Peng, J.B., Sun, X.H., Lu, Q.Z., Meng, L.C., He, H.Q., Qiao, J.W. and Wang, F.Y. (2020), "Characteristics and mechanisms for origin of earth fissures in Fenwei basin, China", *Eng. Geol*., **266**. https://doi.org/10.1016/j.enggeo.2019.105445.

Pacheco-Martínez, J., Hernandez-Marín, M., Burbey, T.J., González-Cervantes, N., Ortíz-Lozano, J.Á., Zermeño-De-Leon, M.E. and Solís-Pinto, A. (2013), "Land subsidence and ground failure associated to groundwater exploitation in the Aguascalientes Valley, México", *Eng. Geol*., **164**(18), 172-186. https://doi.org/10.1016/j.enggeo.2013.06.015.

Sancio, R.B., Bray, J.D., Stewart, J.P., Youd, T.L., Durgunoğlu, H.T., Önalp, A., Seed, R.B., Christensen, C., Baturay, M.B. and Karadayılar, T. (2002), "Correlation between ground failure and soil conditions in Adapazari, Turkey", *Soil Dyn. Earthq. Eng*., **22**(9-12), 1093-1102. https://doi.org/10.1016/S0267-7261(02)00135-5.

Stacey, T.R. and Bell, F.G. (1999), "The influence of subsidence on planning and development in Johannesburg, South Africa", *Environ. Eng. Geosci*., **5**(4), 373-388. https://doi.org/10.2113/gseegeosci.V.4.373.

Wang, G.Y., You, G., Shi, B., Qiu, Z.L., Li, H.Y. and Tuck, M. (2010), "Earth fissures in Jiangsu Province, China and geological investigation of Hetang earth fissure", *Environ. Earth Sci*., **60**(1), 35-43. https://doi.org/10.1007/s12665-009-0167-5.

Wan, J.W., Li, B., Tan, C.X., Feng, C.J., Zhang, P. and Qi, B.S. (2020), "Characteristics and main causes of earth fissures in northeastern Beijing Plain, China", *Bull. Eng. Geol. Environ*., **79**, 2919-2935. https://doi.org/10.1007/s10064-020-01731-z.

Wang, F.Y., Peng, J.B., Chen, Z.X., Wang, Q.L., Meng, Z.J., Qiao, J.W. and Zhao, J.Y. (2020), "Development characteristics and mechanisms of damage-causing urban ground fissures in Datong City, China", *Eng. Geol*., **271**, 1-10. https://doi.org/10.1016/j.enggeo.2020.105605.

Wang, J.M. (2000), Theory of ground fissures hazard and its application, Shaanxi Science and Technology Press: Xi'an. (in Chinese)

Wei, Y.C., Lee, C.J., Hung, W.Y. and Huei-Tsyr, C. (2010), "Application of Hilbert-Huang transform to characterize soil liquefaction and quay wall seismic responses modeled in centrifuge shaking-table tests", *Rock Soil Mech*., **30**(7), 614-629. https://doi.org/10.1016/j.soildyn.2010.02.005.

Wang, Q.Y., Hu, Z.P., Wang, R. and Luo, L.J. (2015), "Shaking table test study on seismic acceleration response of fissure sites under horizontal seismic action", *J. China Railway Soc*., **37**(12), 121-128. (in Chinese).

Xiong, Z.M., Chen, X., Zhang, C., Huo, X.P. and Zhuge, Y. (2018), "Shaking table tests of RC frame structure across the earth fissure under earthquake", *Struct. Des. Tall Spec. Build*., **27**(14), 9-29. https://doi.org/10.1002/tal.1496.

Xiong, Z.M., Zhang, C., Huo, X.P. and Ochoa, J.J. (2020), "Distributing disciplinarian of ground motion parameters on an earth fissures site during strong earthquakes", *Earthq. Eng. Eng. Vib*., **19**(3), 597-610. https://link.springer.com/article/10.1007/s11803-020-0583-9.

Xuan, Y., Deng, Y.H., He, J., Jiang C., Yan, Z.F. and Wu, W. (2021), "Microtremor-based analysis of the dynamic response characteristics of earth-fissured sites in the Datong basin, China", *Earthq. Eng. Eng. Vib*., **20**(3), 567-582. https://doi.org/10.1007/s11803-021-2039-2.

Zhang, J.M. (1990), Research on Ground Fissures in Xi'an City. Northwest University Press, Xi'an, (in Chinese).

Zhu, C.Q., Cheng, H.L., Bao, Y.J., Chen, Z.Y. and Huang, Y. (2022), "Shaking table tests on the seismic response of slopes to near-fault ground Motion", *Geomech. Eng*., **29**(2), 133-143. https://doi.org/10.12989/gae.2022.29.2.133

GC